Earth, Planets and Space

FULL PAPER Open Access

Global marine gravity anomalies from multi-satellite altimeter data

Xiaoyun Wan[1], Ruijie Hao[1], Yongjun Jia[2*], Xing Wu[3], Yi Wang[4] and Lei Feng[4]

Abstract

In this study, China's first altimeter satellite Haiyang-2A (HY-2A) data combined observations from CryoSat-2, SARAL/AltiKa, and Jason-1&2 are used to calculate the global (60°S–60°N) marine deflections of the vertical and gravity anomalies named Global Marine Gravity Anomaly Version 1(GMGA1), with grid resolution of $1' \times 1'$. The deflections of the vertical from each satellite observations are first derived from the gradients of the geoid height through the least squares method. The deflections of the vertical are then merged by assigning different weights to each satellite product based on their accuracy. Finally, gravity anomalies are obtained by the remove-restore method. The results reveal that the fused deflections of the vertical have an accuracy of 0.4 arcsec in the north component and 0.8 arcsec in the east component. HY-2A's contribution to the north component of the integrated deflections of the vertical is second only to Cryosat-2. Jason-1/2 accounts for a large proportion of the integrated east components. Compared to worldwide products such as DTU17, Sandwell & Smith V31.1, as well as values from EGM2008, EIGEN-6C4 and XGM2019e_2159, GMGA1 has an accuracy of around 3.3 mGal. By not using HY-2A data, the precision of GMGA1 is reduced by about 0.1 mGal. To further improve the accuracy, seafloor topography information is used to provide short wavelength gravity anomaly. It is verified in the South China Sea (112°E–119E°, 12°N–20°N) using the Parker formula. By combining shipborne depth generated data and GMGA1 through a filtering technique, a new version of gravity anomaly grid with an accuracy improvement of 0.4 mGal in the South China Sea is obtained.

Keywords: Satellite altimetry, Deflections of the vertical, HY-2A, Gravity anomaly

*Correspondence: jiayongjun@mail.nsoas.org.cn

[2] National Satellite Ocean Application Service, Beijing 100081, China
Full list of author information is available at the end of the article

Graphical Abstract

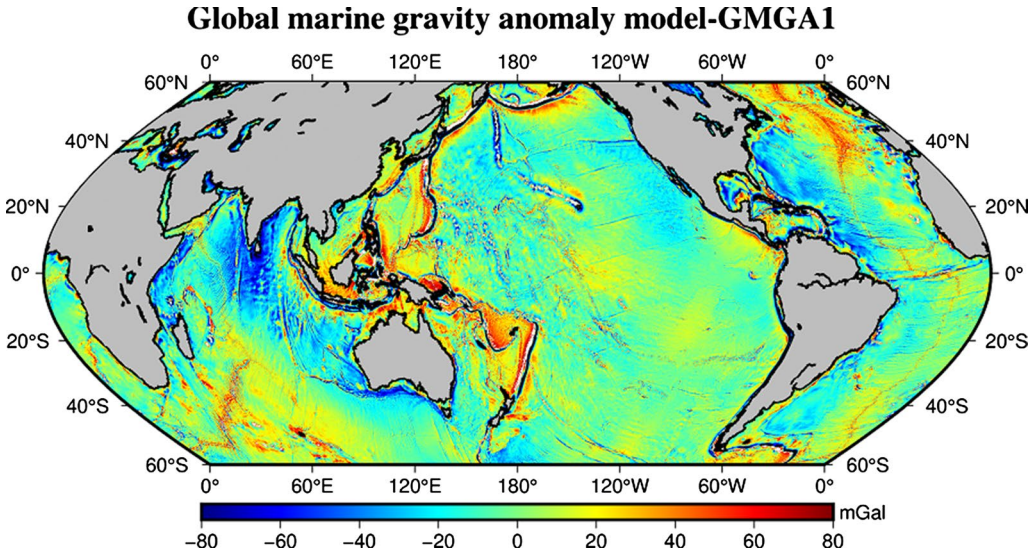

Introduction

With the advance in space technology, altimetry observations have played a significant role in Earth science (Guo et al. 2022a), such as the monitoring of sea level variation (Ablain et al. 2015; Rose et al. 2019; Watson et al. 2015), investigation on ocean geology and plate tectonics (Hwang and Chang 2014; Li et al. 2020; Sandwell and Smith 2009; Sandwell et al. 2014) inversion of marine gravity anomaly (Andersen et al. 2010; Annan and Wan, 2021; Hwang 1998; Sandwell et al. 2013, 2021) and seafloor topography (Annan and Wan 2020; Hu et al. 2021; Smith and Sandwell 1994; Tozer et al. 2019).

The accuracy of the marine gravity anomaly inversion from satellite altimetry observations mainly depends on the density of the observation points, orbit determination precision, the ranging precision of the altimeter, and kinds of corrections (Sandwell et al. 2013; Zhang et al. 2017). After removing the influence of mean dynamic topography (MDT) from the sea surface height (SSH) data, the geoid heights can be obtained, and then the marine gravity anomaly can be deduced according to the inverse Stokes formula (Andersen et al. 2010; Olgiati et al. 1995); The deflections of the vertical can also be used to derive marine gravity using inverse Vening–Meinesz formula (Hwang 1998; Hwang et al. 2002), least squares coordination (LSC) method (Hwang and Parsons 1996), or Laplace's equation (Sandwell and Smith 1997). The deflections of the vertical can be obtained from the geoid gradients calculated from two continuous sea surface height data along the orbit, which can weaken the long wavelength errors (Hwang et al. 2002).

China launched Haiyang-2A (HY-2A) satellite in 2011 and changed its orbit in 2016 to conduct the geodetic mission (GM) for detecting marine gravity anomaly. During its whole lifetime, more than 4 years of GM observations have been obtained. Several investigations have proved that the HY-2A has close accuracy to other altimetry satellites (Jiang et al. 2019; Liu et al. 2020; Wan et al. 2020; Zhang et al. 2020; Zhu et al. 2019; Ji et al. 2021; Guo et al. 2022b), and thus the data of this satellite has a large potential in Earth science, including global marine gravity anomaly inversion. However, few global marine gravity anomaly products are derived using HY-2A observations. Although Wan et al. (2020) has derived global gravity products using HY-2A observations, only part of HY-2A/GM observations was used. The accuracy of products given by Wan et al. (2020) is only around 7–8 mGal, and the grid size is $0.5^{\circ} \times 0.5^{\circ}$, which is not enough for most Earth science researches. One of the main reasons leading to the not high accuracy in Wan et al. (2020), is that the remove-restored method is not used. Indeed, the remove-restored method is the standard procedure in the derivation of global marine gravity anomaly products such as DTU (Technical University of Denmark) series gravity anomaly products and Sandwell & Smith (S&S) products released by Scripps Institution of Oceanography (SIO). In addition, adding more observations of HY-2A would also improve the accuracy of Wan et al. (2020) results.

In this study, all the observations of HY-2A/GM are used together with CryoSat-2, SARAL/AltiKa-Drifting Phase (SRL/DP), Jason-1/GM, and Jason-2/GM

observations to derive a global version of gravity anomaly with grids size of $1' \times 1'$, called Global Marine Gravity Anomaly Version 1 (GMGA1) in this study. "Method" Section introduces the methods for computing deflections of the vertical and gravity anomaly; "Altimetrydata" Section describes the altimetry data used, and "Results and analysis" Section presents the obtained gravity field products and evaluates their accuracy as well as the contribution from HY-2A observations. To further improve the accuracy of GMGA1, "Discussion" Section discusses the feasibility of the construction of short wavelength gravity anomaly from seafloor topography information. Conclusions are finally drawn in "Conclusion" Section.

Methods

Computation of SSHs

The calculation of SSH with the original data of altimetry satellite needs to go through kinds of corrections, including dry troposphere correction, wet troposphere correction, ionosphere correction, sea tide correction, polar tide correction, solid earth tide correction, dynamic atmosphere correction, and sea state bias, as shown in formulas (1). It is also necessary to eliminate the observed outliers caused by environmental factors, and the observations with values beyond the ranges shown in Table 1 are eliminated:

$$\mathrm{SSH} = \mathrm{altitude} - \mathrm{range\text{-}corrections} \tag{1}$$

in which *altitude* refers to the satellite height above the reference ellipsoid surface, which is provided by the orbit position determination system, and *range* denotes the distance between satellite centroid and sea surface which is provided by the payload altimeter; *corrections* are kinds of correction values.

Computation of deflections of the vertical

The calculation of deflections of the vertical requires geoid data (Hwang et al. 2002). The geoid heights are obtained by deducting the influence of mean dynamic topography (MDT) from SSH data, as shown in formula (2). In this study, the mean dynamic topography DTU15MDT released by DTU is adopted (Knudsen et al. 2016). The deflections of the vertical along the orbit are calculated by two consecutive sampling points along the satellite trajectory, as shown in Eq. (3), and the azimuth between the two points also can be calculated:

$$N_a = \mathrm{SSH}_a - \mathrm{MDT}_a \tag{2}$$

$$\partial h = -\frac{N_b - N_a}{d} \tag{3}$$

Table 1 Editing criteria of altimeter products

Term	Range
SSH (m)	[− 130, 100]
Ionospheric correction (m)	[− 0.4, 0.04]
Sea state bias correction (m)	[− 0.5, 0]
Earth tide correction (m)	[− 1, 1]
Pole tide correction (m)	[− 0.15, 0.15] (for GDR) [− 15, 15] (for L2P)
Oceanic tide correction (m)	[− 5, 5]
Dry tropospheric correction (m)	[− 2.5, − 1.9]
Wet tropospheric correction (m)	[− 0.5, − 0.001]
Dynamic atmospheric correction (m)	[− 2, 2]
Nb measurements of range	Greater than 10 (for GDR) Greater than 10 to 20 (for L2P)
RMS of the range (m)	[0, 0.2]
Significant wave height (m)	[0, 11] (for GDR) [0, 15] (for L2P)
Backscatter coefficient (dB)	[7, 30]
Wind speed (m/s)	[0, 30]
Square off-nadir angle (deg^2)	[− 0.2, 0.64] (for GDR) [− 0.36 ~ 0, 0.09 ~ 0.64] (for L2P)
Nb measurements of backscatter coefficient	Greater than 10
RMS of the backscatter coefficient (dB)	[0, 1]

GDR Geophysical Data Record

Level-2 + (L2P)

where d denotes the spherical distance between points of N_b and N_a; ∂h is the deflection of the vertical along the orbit.

The continuous curvature spline interpolation method (Smith and Wessel 1990) is used to grid the deflections of the vertical by GMT (generic mapping tools) software (Wessel et al. 2019), and the sine and cosine values of the azimuth along the track with grid size of $1' \times 1'$. And then, in the grid with size of $4' \times 4'$, the north and east components of deflections of the vertical can be obtained by the least squares method (Hwang et al. 2002), as shown in Eq. (4):

$$\partial h_j + v_j = \xi \cos\alpha_j + \eta \sin\alpha_j \quad j = 1, 2, 3, \ldots, n \tag{4}$$

In which, ξ denotes the north component of the deflection of the vertical, whereas η is the east component; α_j represents the azimuth of the orbit; v_j means the residual values, n is the total number of grid points.

The deflections of the vertical of five altimetry satellites are fused by a weighting method. The index m represents different deflections of the vertical. The weight, denoted as p_m, is assigned in terms of inverse proportion to the square value of the error standard deviation of deflections of the vertical (denoted as δ_m), as shown

in Eq. (5). Four high-precision models (EGM2008 (Pavlis et al. 2012), EIGEN-6C4 (Foerste et al. 2014), XGM2019e_2159 (Zingerle et al. 2020), S&S V31.1 (https://topex.ucsd.edu/pub/archive/grav/) are used to evaluate the accuracy of deflections of the vertical and the error standard deviations are derived correspondingly. We use the average of error standard deviations, denoted as δ_m in Eq. (5), to derived the weight of each satellite:

$$p_m = \frac{a}{\delta_m^2},\ m = 1,2,3,4,5 \tag{5}$$

where

$$a = \frac{1}{\sum_{m=1}^{5} \frac{1}{\delta_m^2}}. \tag{6}$$

Computation of gravity anomalies

The inversion of gravity anomaly by deflections of the vertical often uses the so-called "remove-restore method". In this study, the 2160° and orders of gravity field model EGM2008 are used as the background field. The residual deflections of the vertical are first obtained by subtracting EGM2008 values from the deflections of the vertical obtained from altimetry satellites, as shown in Eq. (7). And then, the residual gravity anomaly can be derived by Eq. (8) (Sandwell and Smith 1997):

$$\begin{cases} \Delta\xi = \xi - \xi_{\mathrm{EGM2008}} \\ \Delta\eta = \eta - \eta_{\mathrm{EGM2008}} \end{cases} \tag{7}$$

$$\Delta g_{\mathrm{res}}(K,0) = \mathrm{ifft}\left(\frac{i}{|K|} g_0 \left[k_x \Delta\xi(K) + k_y \Delta\eta(K) \right] \right) \tag{8}$$

where

$$\begin{cases} K = (k_x, k_y) \\ k_x = \dfrac{1}{\lambda_x} \\ k_y = \dfrac{1}{\lambda_y} \\ |K| = \sqrt{k_x^2 + k_y^2} \end{cases} \tag{9}$$

in which g_0 is the mean normal gravity, λ_x and λ_y represent the wavelengths of the deflections of the vertical in x and y axes; ifft denotes inverse fast Fourier transform. Finally, gravity anomaly, denoted as Δg, can be recovered by adding the residual gravity anomalies to the values from EGM2008 as Eq. (10):

$$\Delta g = \Delta g_{\mathrm{res}} + \Delta g_{\mathrm{EGM2008}} \tag{10}$$

Altimetry data

In this study, five satellite observations are used, including CryoSat-2, SRL/DP, Jason-1&2/GM, and HY-2A/GM. Data of CryoSat-2, SRL/DP, Jason-1/GM, and HY-2A/GM are provided by AVISO (Archiving, Validation, and Interpretation of Satellite Oceanographic, ftp://ftp-access.aviso.altimetry.fr/uncross-calibrated/open-ocean/non-time-critical/l2p/sla), i.e., 1 Hz Along-track L2P altimeter data (CNES 2020). GDR of Jason-2/GM is used from ftp://@ftp-access.aviso.altimetry.fr/geophysical-data-record/jason-2. The detailed information on the used data is shown in Table 2. The ground tracks of five satellites in western Pacific Ocean (150°E–170°E, 0°–10°N) are shown in Fig. 1.

Results and analysis

Deflections of the vertical

According to the method introduced in "Method" Section, two components of deflections of the vertical of the five altimetry satellites are obtained with grids of $1' \times 1'$. The accuracies of them are evaluated by the comparison with values from highly accurate ultra-high degree gravity field models from the International Centre for Global Earth Models (ICGEM, http://icgem.gfz-potsdam.de/calcgrid), including EGM2008,

Table 2 Altimetry data information

Satellite	Product	Inclination (°)	Cycle duration (days)	Time period
CryoSat-2	L2P	92	369	10.07–20.05 (cycle7–cycle130)
SRL /DP	L2P	98.55	35 (virtual cycle)	16.07–21.04 (cycle100–cycle149)
Jason-1/GM	L2P	66	406	12.05–13.06 (cycle500–cycle537)
Jason-2/GM	GDR	66	406	17.07–19.10 (cycle500–cycle644)
HY-2A/GM	L2P	99.34	168	16.04–20.06 (cycle121–cycle288)

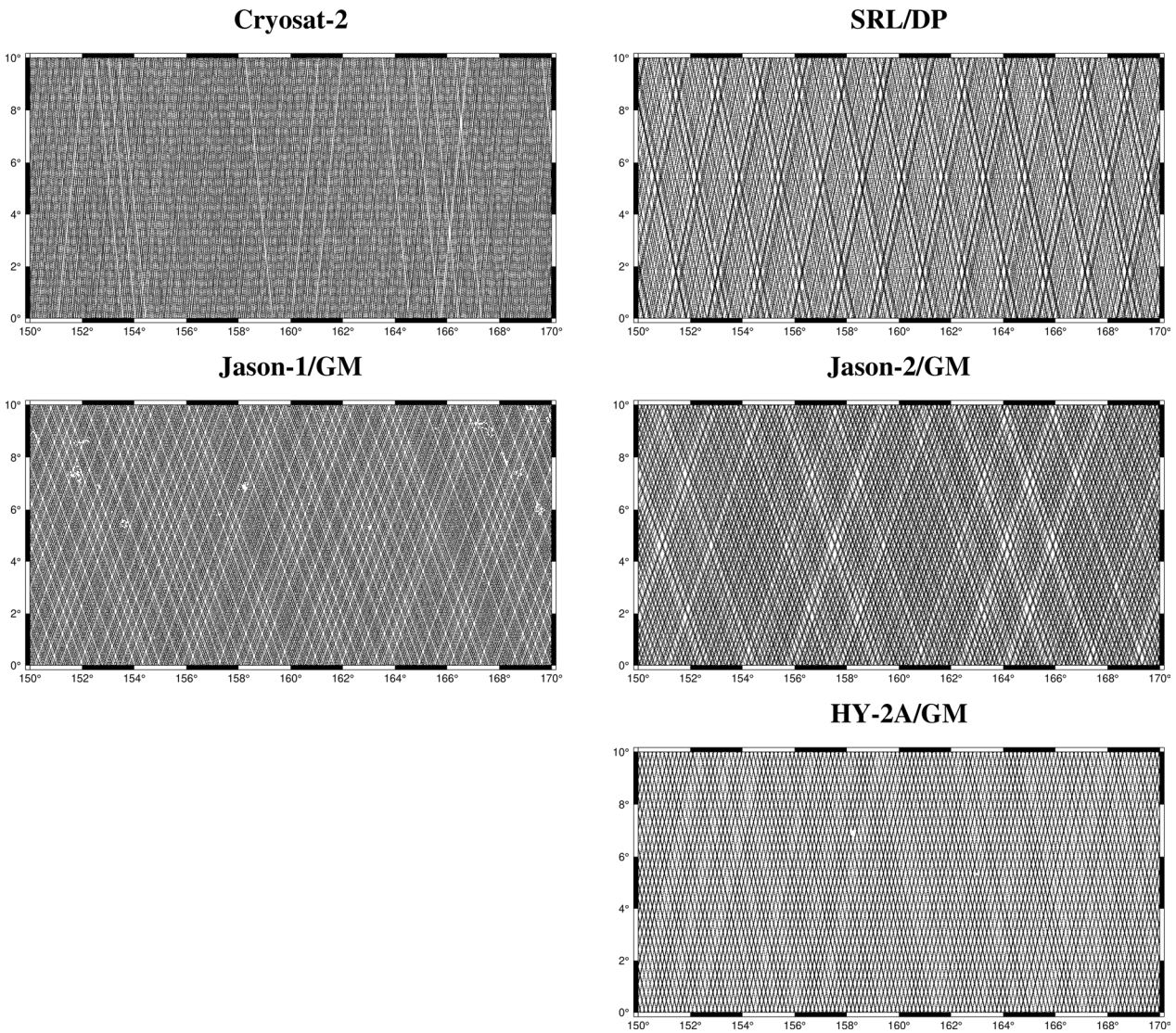

Fig. 1 Ground tracks of five satellites

EIGEN-6C4 and XGM2019e_2159, and deflections of the vertical released by SIO, i.e., S&S V31.1. Table 3 presents the statistical results of the comparison.

According to Table 3, it is easy to find that all the east component of deflections of the vertical has an obviously poorer accuracy than the north one. This is because to expand the earth observation coverage, the inclination angle of altimetry satellite is usually designed to be close to 90°, which affects the calculation of deflections of the vertical, resulting in the accuracy of the east component being several times lower than that of north component (Annan and Wan 2021; Sandwell and Smith 1997; Wan et al. 2020). Because the Cryosat-2 data have high observation accuracy, long period, dense sampling points, and the orbit inclination of the satellite is closest to 90°, the accuracy of the north component of deflections of the vertical from by Cryosat-2 is the highest, i.e., 0.5 arcsec. In contrast, the east component has the lowest accuracy. The accuracy of the north component of deflections of the vertical calculated by HY-2A has a little better performance than SARAL/AltiKa. The accuracy of the east component of deflections of the vertical calculated by SARAL/AltiKa is second only to Jason-1 and Jason-2. Jason-1 and Jason-2 are two inclined orbit satellites with an orbital inclination of 66°. This leads to the fact the east component of deflections of the vertical calculated by observations of these two satellites has higher accuracy

Table 3 Accuracy statistics of deflections of the vertical from the five altimetry satellites in global marine area (Latitude: − 60°− 60°, Longitude: 0°− 360°) (unit: arcsec)

Satellite	The "True" model	ξ component		η component	
		Mean	STD	Mean	STD
CryoSat-2	EIGEN-6C4	− 0.004	0.507	0.017	3.003
	XGM2019e_2159	− 0.004	0.498	0.016	2.996
	EGM2008	− 0.004	0.478	0.017	2.999
	S&S V31.1	0.004	0.482	0.017	2.990
SRL/DP	EIGEN-6C4	− 0.005	0.641	− 0.004	1.914
	XGM2019e_2159	− 0.004	0.637	− 0.004	1.907
	EGM2008	− 0.005	0.619	− 0.003	1.906
	S&S V31.1	0.004	0.618	− 0.003	1.896
Jason-1/GM	EIGEN-6C4	− 0.004	0.952	− 0.001	1.318
	XGM2019e_2159	− 0.004	0.932	− 0.001	1.286
	EGM2008	− 0.004	0.938	0.000	1.307
	S&S V31.1	0.004	0.933	0.000	1.297
Jason-2/GM	EIGEN-6C4	− 0.004	0.956	0.004	1.329
	XGM2019e_2159	− 0.003	0.950	0.003	1.317
	EGM2008	− 0.004	0.941	0.004	1.318
	S&S V31.1	0.005	0.934	0.004	1.306
HY-2A/GM	EIGEN-6C4	− 0.004	0.635	− 0.003	2.406
	XGM2019e_2159	− 0.004	0.633	− 0.003	2.400
	EGM2008	− 0.005	0.613	− 0.003	2.400
	S&S V31.1	0.004	0.619	− 0.003	2.398

than that of the other three satellites, with an accuracy of about 1.3 arcsec.

Based on the results of Table 3, the average error STD (δ_m in Eq. (5)) of deflections of the vertical of five altimetry satellites is calculated and further used to define the weights (see Eq. (5)) for the fusion of all the satellite results. Table 4 presents the weights of each satellite value. In the north component of deflections of the vertical, Cryosat-2 accounts for 36.1%, followed by HY-2A, and 22.30%; In the east component, Jason-1 and Jason-2 account for 34.2% and 33.4%, respectively. The accuracy evaluation of the weighted fused results is given in Table 5. According to this table, the accuracy of the north component is about 0.4 arcsec, and the accuracy of the east component is about 0.8 arcsec. The accuracy of the fusion result is obviously better than that of any single satellite product. For example, compared with Cryosat-2 which has the best performance in the north component, the accuracy of north component is improved by about 0.1 arcsec, and east component is improved by more than 2.0 arcsec; Compared with Jason 1 or 2, which has best performance in the east component, the accuracies of the deflections of the vertical are improved 0.5 arcsec in the both two components. Figure 2 shows the spatial distribution of the fused deflections of the vertical.

Table 4 Average error STD and weights of each satellite observations

Satellite	Component	Average STD (arcsec)	Weight
CryoSat-2	ξ	0.491	0.361
	η	2.997	0.065
SRL/DP	ξ	0.628	0.220
	η	1.906	0.159
Jason-1/GM	ξ	0.939	0.099
	η	1.302	0.342
Jason-2/GM	ξ	0.945	0.097
	η	1.318	0.334
HY-2A/GM	ξ	0.625	0.223
	η	2.401	0.100

Gravity anomalies

GMGA1 is obtained by the remove-restore method, as shown in Fig. 3. This study adopts five versions of gravity anomaly products to evaluate the accuracy of GMGA1, and the comparison results are given in Table 6. Except for EIGEN-6C4, the STD of the differences between GMGA1 and the other four models are all about or smaller than 3.3 mGal.

Assuming gravity anomalies of S&S V31.1 are the true values, the spatial distribution of GMGA1 errors is shown in Fig. 4. Comparing Figs. 3 and 4, it is easy to find that significant errors usually exist in the regions, where gravity anomaly varies largely. We conduct statistics on the error variations with ocean water depths. The ocean water depths data are provided by SRTM15 + V2.0, which is given as grids of 15″ (~ 500 m) and has high accuracy (Hao et al. 2022; Tozer et al. 2019). The abscissa interval in Fig. 5 is 500 m. The error tends to decrease first and then increase in error STD. The accuracy is high in 3500–6500 m water depth. It seems there is a systematic error

Table 5 Accuracy evaluation results of the fused deflections of the vertical (unit: arcsec)

Difference	Component	Max.	Min.	Mean	STD
Fusion-EIGEN-6C4	ξ	17.145	− 14.002	− 0.004	0.427
	η	10.427	− 12.424	0.001	0.834
Fusion-XGM2019e_2159	ξ	18.061	− 13.935	− 0.004	0.415
	η	17.172	− 14.479	0.001	0.804
Fusion-EGM2008	ξ	13.330	− 14.750	− 0.004	0.392
	η	8.967	− 10.647	0.002	0.816
Fusion-S&S V31.1	ξ	26.964	− 33.757	0.004	0.393
	η	26.184	− 28.264	0.002	0.798

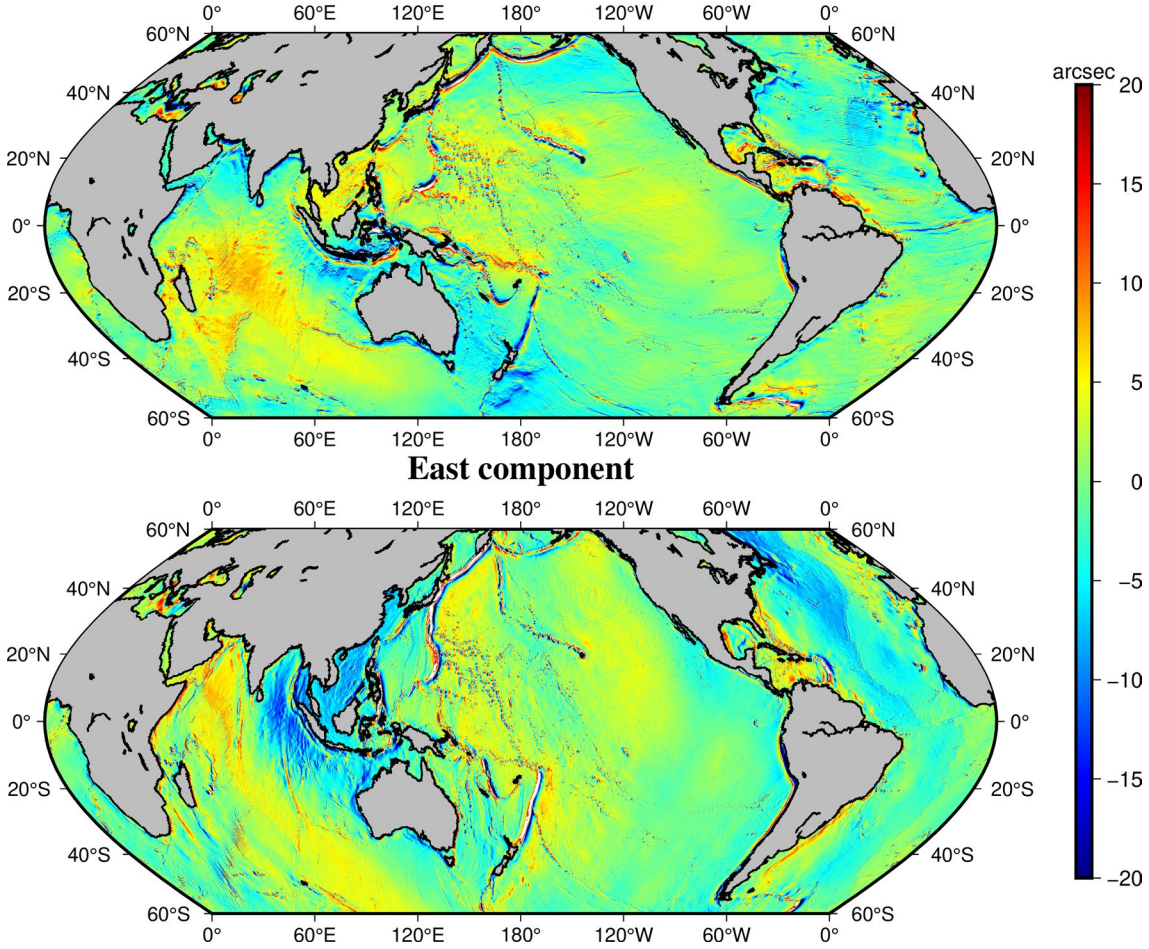

Fig. 2 Fused deflections of the vertical

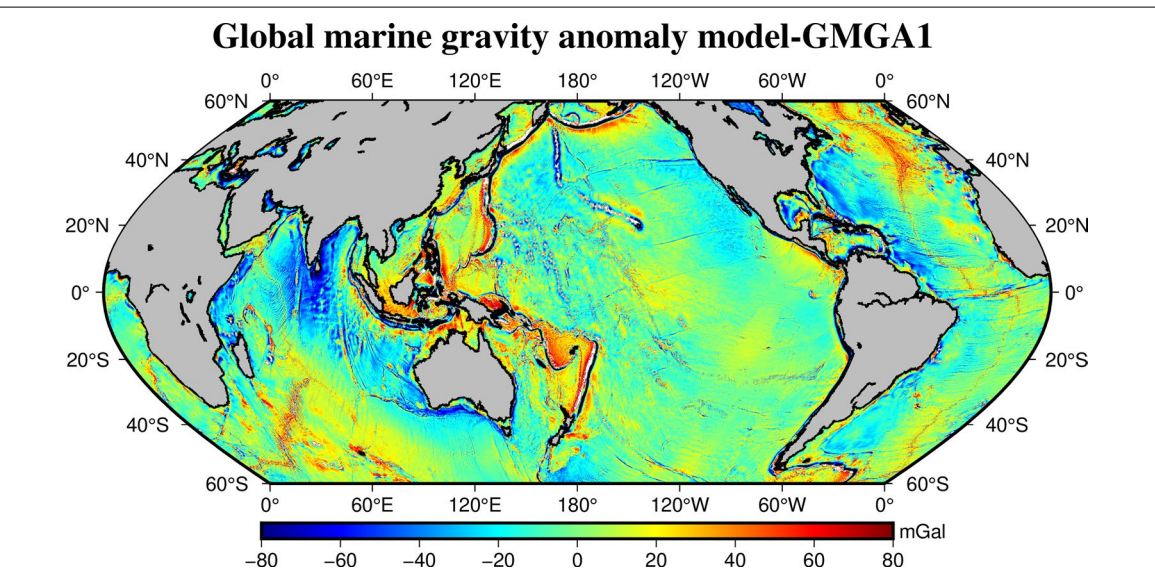

Fig. 3 Inverted gravity anomaly model

Table 6 Accuracy evaluation results of GMGA1 (unit: mGal)

Different	Max.	Min.	Mean	STD
Fusion—EIGEN-6C4	88.558	− 62.661	− 0.000	3.513
Fusion—XGM2019e_2159	79.982	− 74.286	0.011	3.338
Fusion—EGM2008	79.337	− 70.754	0.002	3.319
Fusion—DTU17	62.872	− 58.347	− 0.001	3.021
Fusion—S&S V31.1	230.956	− 209.845	0.123	3.253

in the deep ocean area in terms of the error mean value. For example, in the region with water depth of more than 7000 m, the average error is greater than 1 mGal. Table 7 shows the ratio of the errors in terms of the magnitude. The results reveal that the data with errors less than 5 mGal account for 90.71%, and the data with errors less than 10 mGal account for 99.21%.

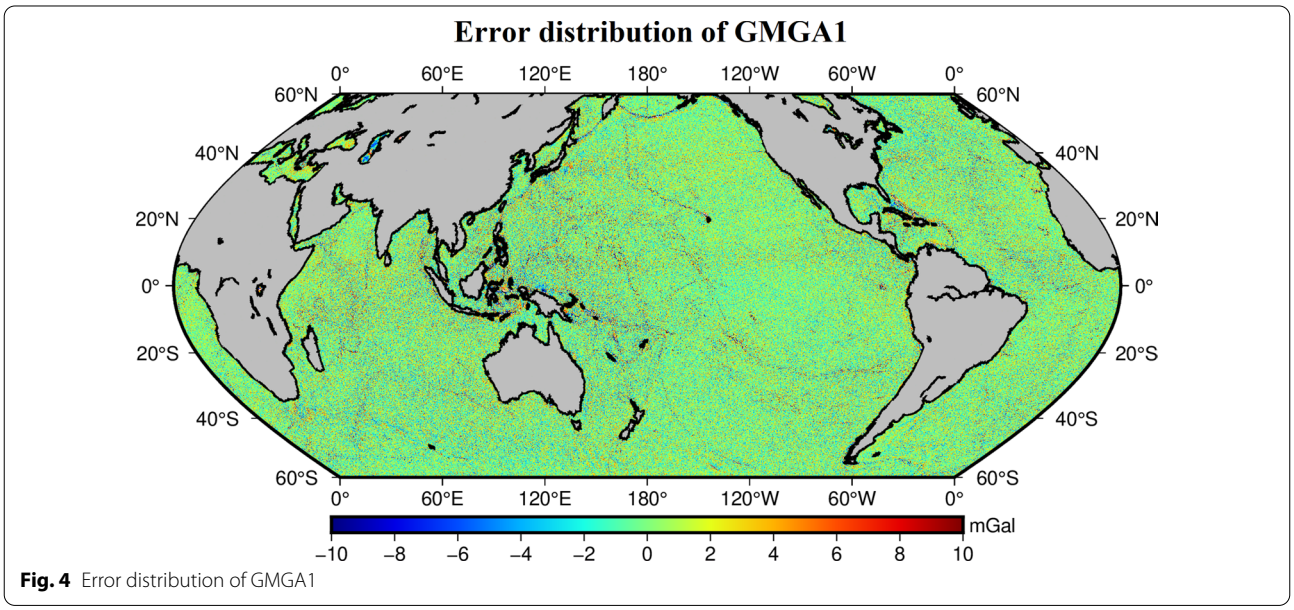

Fig. 4 Error distribution of GMGA1

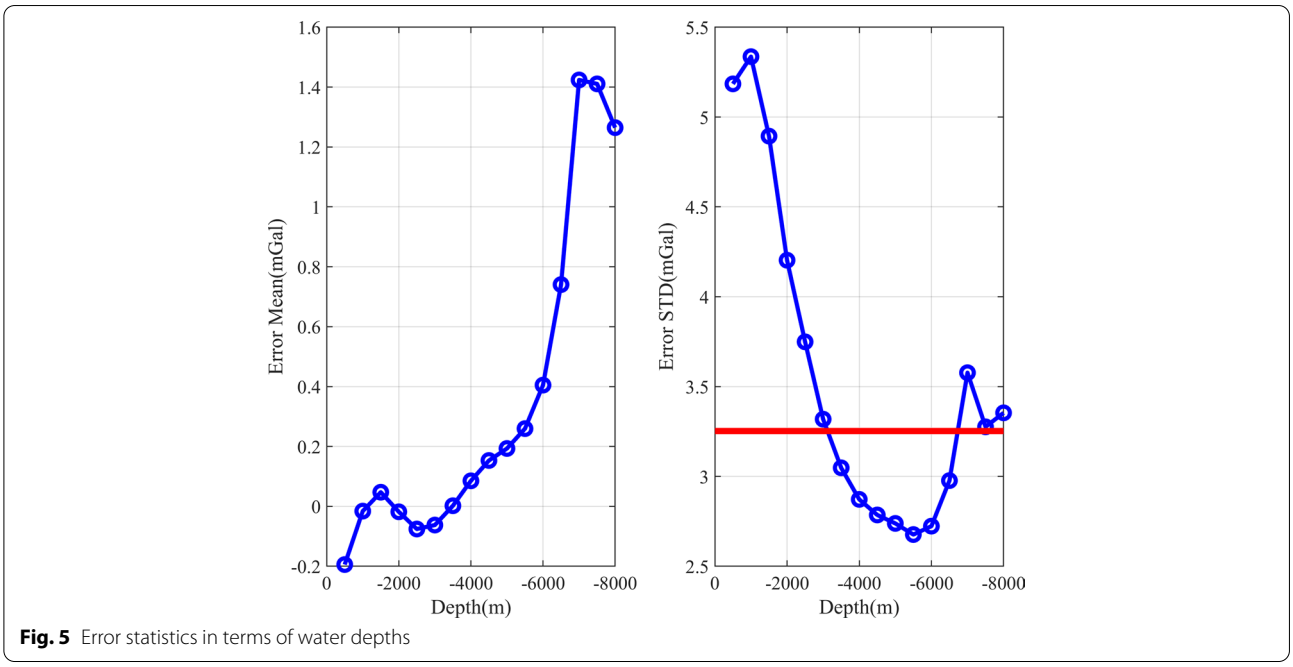

Fig. 5 Error statistics in terms of water depths

Table 7 Error ratio statistics

Index (mGal)	< 1	< 2	< 3	< 4	< 5	< 6	< 7	< 8	< 9	< 10
Percent (%)	28.14	52.52	70.94	83.26	90.71	94.88	97.09	98.25	98.86	99.21

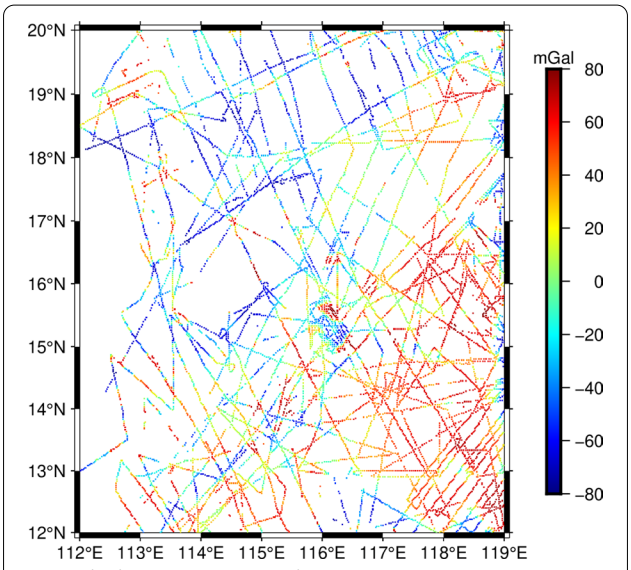

Fig. 6 Shipborne gravity anomalies

Table 8 Accuracy evaluation using shipborne and airborne gravity observations (unit: mGal)

Difference	Max	Min	Mean	STD
GMGA1—shipborne gravity				
Before removing gross errors	23.170	− 24.137	− 0.273	5.967
After removing gross errors	17.188	− 17.729	− 0.256	5.826
GMGA1—airborne gravity				
Before removing gross errors	63.893	− 35.697	0.643	3.586
After removing gross errors	8.924	− 7.317	0.804	2.707

GMGA1 was evaluated in the South China Sea (112°E–119°E, 12°N–20°N) using the shipborne gravity provided by NCEI (National Centers for Environmental Information, https://www.ngdc.noaa.gov/ngdc.html), as shown in Fig. 6. First of all, it is needed to delete the gross error of the shipborne data, and the data which deviates from the EGM2008 model by 15 mGal are deleted, and the amount of remaining data is 90461. Taking the shipborne data as the true value, the error STD of GMGA1 in this area is 5.967 mGal (see Table 8), after removing the points, where the errors deviate from the mean error by three times the initial error STD, the error standard deviation is 5.826 mGal.

Table 9 Weight distribution without HY-2A data

Satellite	Component	Average STD (arcsec)	Weight
CryoSat-2	ξ	0.491	0.464
	η	2.997	0.072
SRL/DP	ξ	0.628	0.284
	η	1.906	0.177
Jason-1/GM	ξ	0.939	0.127
	η	1.302	0.380
Jason-2/GM	ξ	0.945	0.125
	η	1.318	0.371

We also adopted the airborne gravity data in the South China Sea to assess the accuracy of GMGA1. The data are provided by the China Aero Geophysical Survey and Remote Sensing Center for Natural Resources with a resolution of 0.36″ (~10 m) in longitude direction and 1.5″ in latitude direction. The amount of the data is 48,01,806, and the location is in the region with latitude of 9°–16°N and longitude of 112°–114°E. To let the two versions of the data be on the same surface, we first conducted a downward continuation to the airborne gravity data by Eq. (11) (Liu et al. 2014):

$$g_h = ifft[e^{2\pi|K|h} G_0(k_x, k_y)] \tag{11}$$

in which k_x and k_y are the wavenumbers; $|K| = \sqrt{k_x^2 + k_y^2}$; h is the height of the airplane; G_0 is the Fourier transform values of the airborne gravity data. Table 8 demonstrates the statistics on the comparison. If the airborne data are treated as true values, the error STD of GMGA1 is 3.586 mGal. The largest error exceeds 60 mGal, which indicates there may exist some gross errors. To reduce the influence of gross errors, the points where the errors deviate from the mean error by three times the initial error STD are removed. The results show that the error STD is reduced to 2.707 mGal after removing the gross errors.

Analysis of HY-2A's contribution

Compared with the mainstream gravity anomaly products released by other institutes, the main difference of this study is the usage of 4 years of HY-2A data. This section analyzing the contribution of HY-2A in the inversion of GMGA1. This is achieved by repeating the inversion without using HY-2A observations and then analyzes the

Table 10 Accuracy comparison of deflections of the vertical derived using and not using HY-2A data (unit: arcsec)

Difference	Component	Using HY-2A data		Without HY-2A data	
		Mean	STD	Mean	STD
Fusion—EIGEN-6C4	ξ	− 0.004	0.427	− 0.004	0.446
	η	0.001	0.834	0.002	0.869
Fusion—XGM2019e_2159	ξ	− 0.004	0.415	− 0.004	0.432
	η	0.001	0.804	0.002	0.839
Fusion—EGM2008	ξ	− 0.004	0.392	− 0.004	0.413
	η	0.002	0.816	0.002	0.852
Fusion—S&S V31.1	ξ	0.004	0.393	0.004	0.411
	η	0.002	0.798	0.002	0.834

Table 11 Accuracy comparison of gravity anomaly derived using and not using HY-2A data (unit: mGal)

Difference	Using HY-2A data		Without HY-2A data	
	Mean	STD	Mean	STD
Fusion—EIGEN-6C4	0.000	3.513	− 0.003	3.629
Fusion—XGM2019e_2159	0.011	3.338	0.009	3.445
Fusion—EGM2008	0.002	3.319	0.000	3.440
Fusion—DTU17	− 0.001	3.021	− 0.003	3.141
Fusion—S&S V31.1	0.123	3.253	0.120	3.362

accuracy variations. The calculation method is the same as that in "Method" Section. Table 9 gives the weight values of deflections of the vertical of each model without using HY-2A data, and Table 10 presents the statistical results on the new fused deflections of the vertical. It can be seen from Table 10 that the accuracy of the north component of deflections of the vertical calculated without using HY-2A data is reduced by about 0.02 arcsec, and the accuracy of the east component is reduced by about 0.03 arcsec. The accuracy of gravity anomaly is reduced by about 0.1 mGal, as shown in Table 11, which is similar to the conclusion obtained by Zhu et al. (2020), i.e., with an improvement of about 0.06 mGal in the South China Sea using HY-2A observations.

Figure 7 shows the spatial distribution of data points, where accuracy has been improved by more than 4 mGal using HY-2A data. According to this figure, most of these data points are located in areas with severe fluctuations of gravity anomalies, and these areas are usually in seamounts and trenches. It indicates that the usage of HY-2A data can improve the gravity detection accuracy in these landforms, which is of great significance for marine research.

Discussion

Due to the limitation of altimetry satellite payloads, orbit parameters and data processing means, altimetry satellites cannot retrieve all the short wavelength signals of gravity anomaly with high precision. Therefore, other methods are needed to recover the short wavelength gravity anomaly. Indeed, the short wavelength gravity anomaly reflects some complex and high-frequency topographic information. A large number of studies (Hu et al. 2020; Hwang 1999; Smith and Sandwell 1997; Sandwell et al. 2014) have shown that there is a linear relationship between the gravity anomaly in the medium and short wavelength part of the sea depth which reflects seafloor topography variations. In theory, seafloor topography must influence the values of gravity anomaly at the sea surface. Conversely, the information of seafloor topography variation provided by ocean

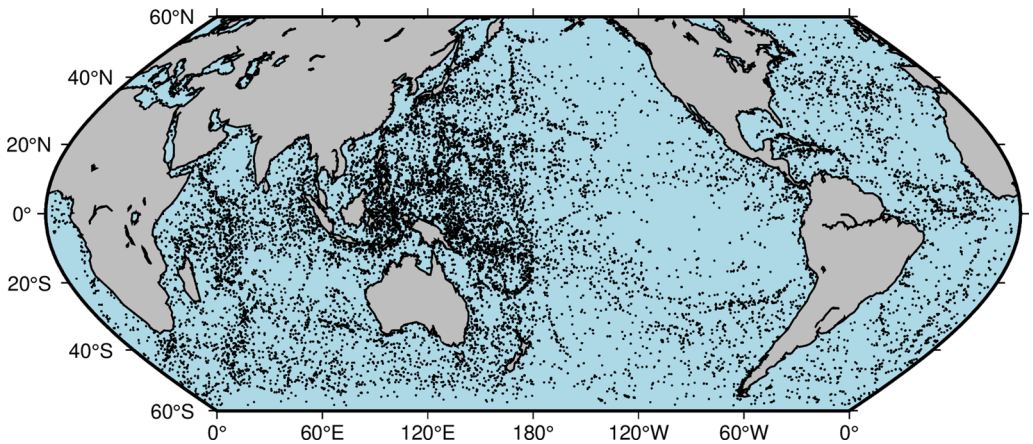

Fig. 7 Distribution of the points, where the accuracy of gravity anomaly is improved by more than 4 mGal

water depth can be used to derive short wavelength gravity anomaly signals, which are not recovered by the altimetry observations. This section discusses this issue.

The study area is located in the South China Sea, with longitude of 112°E–119°E and latitude of 12°N–20°N. To represent seafloor topography with as high accuracy as possible, this study experiments with depth data from NECI shipborne bathymetry (https://www.ncei.noaa.gov/maps/bathymetry/) and three other versions of bathymetry models, including ETOPO1 (https://www.ngdc.noaa.gov/mgg/global/global.html), SRTM15+V2.0 (https://topex.ucsd.edu/pub/archive/srtm15/V2/) and DTU18 (https://ftp.space.dtu.dk/pub/DTU18/1_MIN/).

According to Parker (1973) and Hu et al. (2020), the gravity anomaly generated by seafloor topography can be approximately expressed as Eq. (12):

$$\Delta G(k)=ifft\left[2\pi G\Delta\rho e^{-2\pi kd}H(k)\right] \tag{12}$$

where $\Delta\rho$ is the density difference between the upper crust and seawater and is set as 1770 kg/m^3 (Hu et al. 2021) in this study; G is gravitational constant; $k=\frac{1}{\lambda}$; λ is the wavelength of the topography; $H(k)$ is the Fourier transform values of water depths; $\Delta G(k)$ is the forward-derived gravity anomaly; d is the mean depth in the region, which is average values of ETOPO1, SRTM15+V2.0, and DTU18, i.e., 3200 m, in this study.

S&S V31.1 data are set as the "true value" to evaluate the accuracy of the derived gravity anomaly. This study adopts a bandpass filter (Wan et al. 2021) to obtain the short wavelength gravity anomaly. Starting from [2 3] km as the first passband, this study takes 1 km as the step to change the filter bands. And then, accuracy statistics are conducted to the filtered results. It is worth noting that the boundary effect caused by the Fourier transform would be generated in the computing shown in Eq. (12). To reduce the boundary effect, the areas actually participating in the accuracy statistics are the region with longitude of 113°E–118°E and latitude of 13°N–19°N. As shown in Fig. 8, the short wavelength gravity anomaly retrieved by shipborne depths has higher accuracy than GMGA1 within the bands of 17 km. Compared to GMGA1, the dominant band of SRTM15+V2.0 is within 22 km. Table 12 shows the accuracy statistics in the range of 2–17 km and 2–22 km. The results demonstrate that SRTM15+V2.0 performs best for providing short wavelength gravity anomalies, followed by DTU18.

We choose shipborne depths for further analysis. It can be seen from Fig. 9 that the inversion result from water depth in the band of 2–17 km is closer to S&S V31.1 than

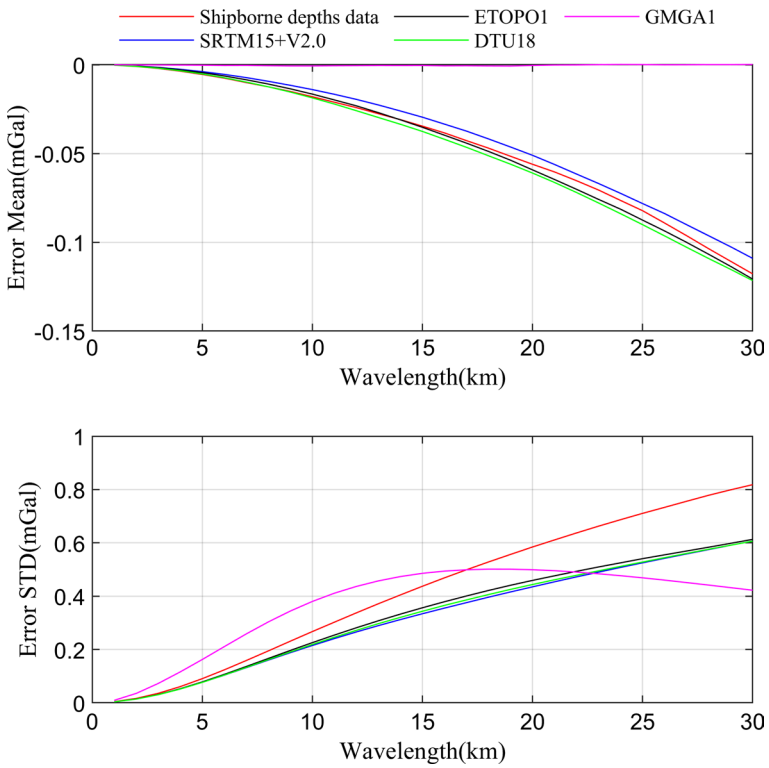

Fig. 8 Accuracy of short wavelength gravity anomaly with variations of wavelengths

Table 12 Accuracy statistics of short wavelength gravity anomaly (unit: mGal)

Difference	2–17 km band		2–22 km band	
	Mean	STD	Mean	STD
Shipborne depths—S&S V31.1	− 0.053	0.795	− 0.084	1.139
SRTM15 + V2.0—S&S V31.1	− 0.041	0.644	− 0.067	0.903
ETOPO1—S&S V31.1	− 0.048	0.674	− 0.079	0.955
DTU18—S&S V31.1	− 0.054	0.653	− 0.086	0.918
GMGA1—S&S V31.1	− 0.001	1.196	− 0.001	1.561

that of GMGA1. Figure 9 also show the error distribution of the two models, i.e., shipborne depths derived values and GMGA1. The errors are mainly concentrated in the area with drastic changes in gravity, and the shipborne depths derived gravity anomaly has obviously smaller errors. Indeed, the region, where gravity varies largely, usually has a large fluctuation of seafloor topography, and thus, it is reasonable to use water depth to improve the short wavelength gravity anomaly.

Although SRTM15 + V2.0, ETOPO1 and DTU18 derived short-wavelength gravity signals have better performance than shipborne depths, if S&S V31.1 is the true value. However, shipborne depths are more direct topography observations than these three models. Especially, the derivations of these three models may have used the information of marine gravity anomaly. Therefore, the signals in the band of 2–17 km are provided by values derived from shipborne depths in this study, and outside of this band are provided by GMGA1. By doing this, a new version of gravity anomaly in the South China Sea is obtained, and the accuracy statistics are given in Table 13. The results reveal that the errors of the new version of gravity anomaly have been reduced by 0.08 mGal in terms of mean value and 0.431 mGal in terms of STD. It verifies the effectiveness of using ocean water depths to improve the accuracy of the short wavelength gravity anomaly.

Conclusions

In this study, deflections of the vertical are first calculated from observations of each of the five altimetry satellites, and then fused using varying weights based on their accuracy. The remove-restore approach is then used to obtain the marine gravity anomaly model, i.e.,

Table 13 Statistics on the accuracy of the new results (mGal)

Difference	Mean	STD
Filter combination model—S&S V31.1	0.154	2.831
GMGA1—S&S V31.1	0.234	3.262

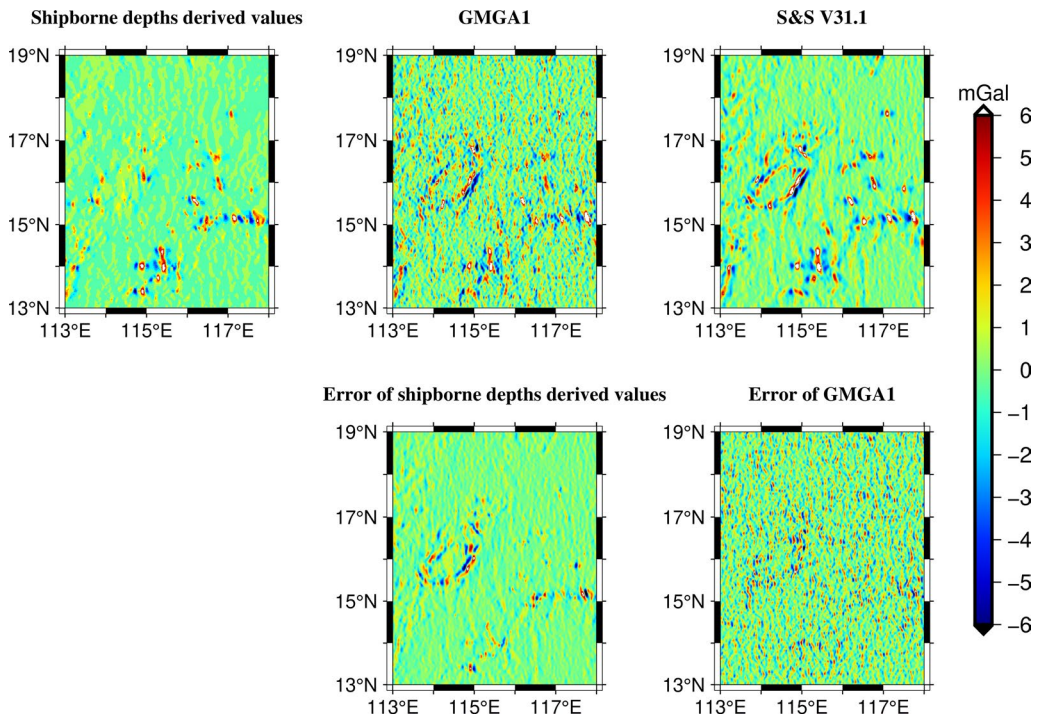

Fig. 9 Gravity anomaly and error in the wavelength range of 2–17 km

GMGA1. Finally, the accuracy of GMGA1 is tested using a variety of products. HY-2A contribution is analyzed, and the effectiveness of using seafloor topography information to enhance the short wavelength gravity anomaly is experimented.

The results demonstrate that CryoSat-2 has the highest accuracy in the north component of deflections of the vertical, while HY-2A is only second to CryoSat-2. Jason-1 and Jason-2 contribute largest to the east component of the fused deflections of the vertical. The fused deflections of the vertical have an accuracy of 0.4 arcsec in the north component and 0.8 arcsec in the east component. Compared to DTU17 and S&S V31.1, GMGA1 has an accuracy of around 3.3 mGal. 90% of the errors are smaller than 5.0 mGal. The accuracy of GMGA1 is also evaluated using airborne gravity observations and the comparison results show that the precision is about 2.7 mGal in the South China Sea. Without using HY-2A data, the precision of gravity anomaly is reduced by about 0.1 mGal; HY-2A can improve the gravity anomaly accuracy in the region, where the signals vary largely.

This study also proved that dense water depth observations could help improve the accuracy of the short wavelength of gravity anomaly. The gravity anomaly derived by shipborne depths data has better accuracy than GMGA1 in the wavelength shorter than 17 km in the South China Sea. The combination results of shipborne depths derived values and GMGA1 improve the accuracy of gravity anomaly by 0.4 mGal in the study area.

Acknowledgements
We would like to thank AVISO for providing the five altimetry satellite observations and China Aero Geophysical Survey and Remote Sensing Center for Natural Resources for providing airborne gravity data. We also want to thank NOAA, ICGEM, SIO, and DTU for providing gravity field products and ocean water depth data.

Author contributions
Conceptualization, XW; data curation, XW, YW and LF; funding acquisition, XW; investigation, XW and RH; methodology, XW, YJ and XW; writing original draft, XW and RH. All author have read and approved the final manuscript.

Funding
This work is funded the by National Natural Science Foundation of China (Nos. 42074017, 41674026).

Availability of data and materials
The data sets used and/or analysed during the current study are available from the corresponding author on reasonable request.

Declarations

Competing interests
The authors declare that they have no competing interests.

Author details
[1]School of Land Science and Technology, China University of Geoscience (Beijing), Beijing 100089, China. [2]National Satellite Ocean Application Service, Beijing 100081, China. [3]Beijing Special Engineering Design and Research Institute, Beijing 100028, China. [4]China Aero Geophysical Survey & Remote Sensing Center for Natural Resources, Beijing 100089, China.

Received: 14 June 2022 Accepted: 13 October 2022
Published online: 08 November 2022

References

CNES (2020) Along-Track Level-2+(L2P) SLA product handbook. https://www.aviso.altimetry.fr/fileadmin/documents/data/tools/hdbk_L2P_all_missions_except_S3.pdf. Accessed 26 Sept 2022

Ablain M, Cazenave A, Larnicol G, Balmaseda MA, Cipollini P, Faugère Y, Fernandes MJ, Henry O, Johannessen JA, Knudsen P, Andersen O, Legeais J, Meyssignac B, Picot N, Roca M, Rudenko S, Scharffenberg MG, Stammer D, Timms G, Benveniste J (2015) Improved sea level record over the satellite altimetry era (1993–2010) from the climate change initiative project. Ocean Sci 11:67–82. https://doi.org/10.5194/os-11-67-2015

Andersen OB, Knudsen P, Berry PAM (2010) The DNSC08GRA global marine gravity field from double retracked satellite altimetry. J Geod 84(3):191–199. https://doi.org/10.1007/s00190-009-0355-9

Annan RF, Wan X (2020) Mapping seafloor topography of Gulf of Guinea using an adaptive meshed gravity-geologic method. Arabian J Geosci 13(7):1–12. https://doi.org/10.1007/s12517-020-05297-8

Annan RF, Wan X (2021) recovering marine gravity over the Gulf of Guinea from multi-satellite sea surface heights. Front Earth Sci. https://doi.org/10.3389/feart.2021.700873

Foerste C, Bruinsma SL, Abrikosov O, Lemoine JM, Schaller T, Goetze HJ, Ebbing J, Marty JC, Flechtner F, Balmino G, Biancale R (2014) EIGEN-6C4. The latest combined global gravity field model including GOCE data up to degree and order 2190 of GFZ Potsdam and GRGS Toulouse. http://icgem.gfz-potsdam.de/Foerste-et-al-EIGEN-6C4.pdf. Accessed 10 Oct 2022

Guo J, Hwang C, Deng X (2022a) Editorial: application of satellite altimetry in marine geodesy and geophysics. Front Earth Sci 10:910562. https://doi.org/10.3389/feart.2022.910562

Guo J, Luo H, Zhu C, Ji H, Li G, Liu X (2022b) Accuracy comparison of marine gravity derived from HY-2A/GM and CryoSat-2 altimetry data: a case study in the Gulf of Mexico. Geophys J Int 230(2):1267–1279. https://doi.org/10.1093/gji/ggac114

Hao R, Wan X, Wang Y, Annan RF (2022) Evaluation of four global bathymetry models by shipborne depths data. J Surv Eng ASCE 148(2):04021033. https://doi.org/10.1061/(ASCE)SU.1943-5428.0000392

Hu M, Zhang S, Jin T, Wen H, Chu Y, Jiang W, Li J (2020) A new generation of global bathymetry model BAT_WHU2020. Acta Geodaetica Et Cartographica Sinica 49(08):939–954. https://doi.org/10.11947/j.AGCS.2020.20190526

Hu M, Li L, Jin T, Jiang W, Wen H, Li J (2021) A new 1′× 1′ global seafloor topography model predicted from satellite altimetric vertical gravity gradient anomaly and ship soundings BAT_VGG2021. Remote Sens 13(17):3515. https://doi.org/10.3390/rs13173515

Hwang C (1998) Inverse Vening Meinesz formula and deflection-geoid formula: applications to the predictions of gravity and geoid over the South China Sea. J Geod 72(5):304–312. https://doi.org/10.1007/s001900050169

Hwang C (1999) A bathymetric model for the South China Sea from satellite altimetry and depth data. Mar Geod 22(1):37–51. https://doi.org/10.1080/014904199273597

Hwang C, Parsons B (1996) An optimal procedure for deriving marine gravity from multi-satellite altimetry. Geophys J Int 125(3):705–718. https://doi.org/10.1111/j.1365-246X.1996.tb06018.x

Hwang C, Chang ETY (2014) Seafloor secrets revealed. Science 346(6205):32–33. https://doi.org/10.1126/science.1260459

Hwang C, Hsu HY, Jang RJ (2002) Global mean sea surface and marine gravity anomaly from multi-satellite altimetry: applications of deflection-geoid and inverse Vening Meinesz formulae. J Geod 76(8):407–418. https://doi.org/10.1007/s00190-002-0265-6

Ji H, Guo J, Zhu C, Yuan J, Liu X, Li G (2021) On Deflections of vertical determined from HY-2A/GM altimetry data in the Bay of Bengal. IEEE J Sel Top Appl Earth Observ Remote Sens 14:12048–12060. https://doi.org/10.1109/JSTARS.2021.3129273

Jiang X, Jia Y, Zhang Y (2019) Measurement analyses and evaluations of sea-level heights using the HY-2A satellite's radar altimeter. Acta Oceanol Sin 38(11):134–139. https://doi.org/10.1007/s13131-019-1503-6
Knudsen P, Andersen O, Maximenko N (2016) The updated geodetic mean dynamic topography model-DTU15MDT. In: Presented at the ESA Living Planet Symposium. Prague, Czech Republic
Li Q, Bao L, Shum CK (2020) Altimeter-derived marine gravity variation studies the submarine plate tectonic motion. Chinese J Geophys 63(07):2506–2515. https://doi.org/10.6038/cjg2020N0436
Liu X, Li Y, Xiao Y, Zhai Z (2014) Optimal regularization parameter determination method in downward continuation of gravimetric and geomagnetic data. Acta Geodaetica Et Cartographica Sinica 43(09):881–887. https://doi.org/10.13485/j.cnki.11-2089.2014.0160
Liu Q, Xu K, Jiang M, Wang J (2020) Preliminary marine gravity field from HY-2A/GM altimeter data. Acta Oceanol Sin 39(7):127–134. https://doi.org/10.1007/s13131-020-1610-4
Olgiati A, Balmino G, Sarrailh M, Green CM (1995) Gravity anomalies from satellite altimetry: comparison between computation via geoid heights and via deflections of the vertical. Bull Geod 69(4):252–260. https://doi.org/10.1007/BF00806737
Parker RL (1973) The rapid calculation of potential anomalies. Geophys J Int 31(4):447–455. https://doi.org/10.1111/j.1365-246X.1973.tb06513.x
Pavlis NK, Holmes SA, Kenyon SC, Factor JK (2012) The development and evaluation of the Earth Gravitational Model (EGM). J Geophys Res Solid Earth. https://doi.org/10.1029/2011JB008916
Rose SK, Andersen OB, Passaro M, Ludwigsen CA, Schwatke C (2019) Arctic Ocean sea level record from the complete radar altimetry era: 1991–2018. Remote Sens 11(14):1672. https://doi.org/10.3390/rs11141672
Sandwell DT, Smith WHF (1997) Marine gravity anomaly from Geosat and ERS 1 satellite altimetry. J Geophys Res Solid Earth 102(B5):10039–10054. https://doi.org/10.1029/96JB03223
Sandwell DT, Smith WHF (2009) Global marine gravity from retracked Geosat and ERS-1 altimetry Ridge segmentation versus spreading rate. J Geophys Res Solid Earth. https://doi.org/10.1029/2008JB006008
Sandwell D, Garcia E, Soofi K, Wessel P, Chandler M, Smith WHF (2013) Toward 1-mGal accuracy in global marine gravity from CryoSat-2, Envisat, and Jason-1. Leading Edge 32(8):892–899. https://doi.org/10.1190/tle32080892.1
Sandwell DT, Müller RD, Smith WHF, Garcia E, Francis R (2014) New global marine gravity model from CryoSat-2 and Jason-1 reveals buried tectonic structure. Science 346(6205):65–67. https://doi.org/10.1126/science.1258213
Sandwell DT, Harper H, Tozer B, Smith WHF (2021) Gravity field recovery from geodetic altimeter missions. Adv Space Res 68(2):1059–1072. https://doi.org/10.1016/j.asr.2019.09.011
Smith WHF, Sandwell DT (1994) Bathymetric prediction from dense satellite altimetry and sparse shipboard bathymetry. J Geophys Res Solid Earth 99(B11):21803–21824. https://doi.org/10.1029/94JB00988
Smith WHF, Wessel P (1990) Gridding with continuous curvature splines in tension. Geophysics 55(3):293–305. https://doi.org/10.1190/1.1442837
Smith WHF, Sandwell DT (1997) Global sea floor topography from satellite altimetry and ship depth soundings. Science 277(5334):1956–1962. https://doi.org/10.1126/science.277.5334.1956
Tozer B, Sandwell DT, Smith WHF, Olson C, Beale JR, Wessel P (2019) Global bathymetry and topography at 15 arcsec: SRTM15+. Earth Planets Space 6(10):1847–1864. https://doi.org/10.1029/2019EA000658
Wan X, Annan RF, Jin S, Gong X (2020) Vertical deflections and gravity disturbances derived from HY-2A Data. Remote Sens 12(14):2287. https://doi.org/10.3390/rs12142287
Wan X, Han W, Ran J, Ma W, Annan RF, Li B (2021) Seafloor density contrast derived from gravity and shipborne depth observations: a case study in a local area of Atlantic Ocean. Front Earth Sci 9:668863. https://doi.org/10.3389/feart.2021.668863
Watson CS, White NJ, Church JA, King MA, Burgette RJ, Legresy B (2015) Unabated global mean sea-level rise over the satellite altimeter era. Nat Clim Chang 5(6):565–568. https://doi.org/10.1038/nclimate2635
Wessel P, Luis JF, Uieda L, Scharroo R, Wobbe F, Smith WHF, Tian D (2019) The generic mapping tools version 6. Geochem Geophys Geosyst 20(11):5556–5564. https://doi.org/10.1029/2019GC008515
Zhang S, Sandwell DT, Jin T, Li D (2017) Inversion of marine gravity anomalies over southeastern China seas from multi-satellite altimeter vertical deflections. J Appl Geophys 137:128–137. https://doi.org/10.1016/j.jappgeo.2016.12.014
Zhang S, Andersen OB, Kong X, Li H (2020) Inversion and validation of improved marine gravity field recovery in South China Sea by incorporating HY-2A altimeter waveform data. Remote Sens 12(5):802. https://doi.org/10.3390/rs12050802
Zhu C, Guo J, Hwang C, Gao J, Yuan J, Liu X (2019) How HY-2A/GM altimeter performs in marine gravity derivation: assessment in the South China Sea. Geophys J Int 219(2):1056–1064. https://doi.org/10.1093/gji/ggz330
Zhu C, Guo J, Gao J, Hwang C, Yu S, Yuan J, Ji B, Guan B (2020) Marine gravity determined from multi-satellite GM/ERM altimeter data over the South China Sea SCSGA V1.0. J Geod 94(5):1–16. https://doi.org/10.1007/s00190-020-01378-4
Zingerle P, Pail R, Gruber T, Oikonomidou X (2020) The combined global gravity field model XGM2019e. J Geod 94(7):1–12. https://doi.org/10.1007/s00190-020-01398-0

Publisher's Note